Proceedings of the XIII International Conference "Ion Implantation and Other Applications of Ions and Electrons"

Effect of Ti6Al4V Substrate Manufacturing Technology on the Properties of PVD Nitride Coatings

M. Walczak*, K. Pasierbiewicz and M. Szala

Lublin University of Technology, Faculty of Mechanical Engineering, Department of Materials Engineering, Lublin, Nadbystrzycka 36, 20-618 Lublin, Poland

Doi: 10.12693/APhysPolA.142.723 *e-mail: m.walczak@pollub.pl

Titanium alloys can be fabricated by additive manufacturing techniques, which makes it possible to produce machine components of complex geometries that would be difficult to produce by standard methods such as machining, forming, and casting. Although titanium alloys have a high strength-to-weight ratio, their tribological characteristics are insufficient. For this reason, ceramic coatings with high tribological properties, e.g., PVD coatings, are frequently deposited on titanium alloys. Still, the surface layer properties of Ti6Al4V alloy produced by the direct metal laser sintering differ from those exhibited by this alloy when produced by the standard means in terms of microstructure, internal stresses, texture, and porosity. In light of the above, the objective of this study was to determine the relationship between the surface layer microstructure, morphology, and mechanical properties of the direct metal laser sintering produced Ti6Al4V alloy and the adhesion of PVD nitride coatings. The test samples of Ti6Al4V alloy were fabricated by two different techniques, i.e., conventional manufacturing from wrought material (in the annealed state) and direct metal laser sintering. Two different PVD coatings, AlTiN and TiAlN, were deposited by magnetron sputtering on a titanium substrate. Internal stresses were measured by the X-ray diffraction and $\sin^2(\psi)$ method. The microstructure was examined by optical microscopy. Coating thickness was measured by the ball crater test. After that, coating nanohardness was measured by the Olivier–Pharr method, and coating/substrate adhesion was assessed by the scratch test method. The results showed that the PVD coatings deposited on the direct metal laser sintering substrate had considerably higher adhesive properties, which resulted primarily from the better fit of the $E_{\mathrm{coating}}/E_{\mathrm{substrate}}$ ratio and higher compressive stresses. Scratch test results demonstrated that all coatings deposited on the direct metal laser sintering substrate had a nearly 25% higher critical load L_{cr} (which was a measure of adhesion) than the same coatings deposited on the conventionally manufactured substrate. In addition to that, the cohesive damage mechanism was observed for the latter.

topics: titanium alloy, additive manufacturing, hard coatings, physical vapour deposition (PVD)

1. Introduction

Thin nitride coatings such as AlTiN and TiAlN are used wherever resistance to wear is important. Although they are often deposited on the carbide and high-speed steel substrates to improve cutting tool life, they can also be deposited on titanium alloys, especially Ti6Al4V [1–5]. This alloy has very good corrosion resistance and a high strength-to-weight ratio. The latter is particularly desirable in aerospace and automotive applications. However, the tribological properties of Ti6Al4V are known to be poor/unsatisfactory, especially under sliding conditions [6–8]. High coefficients of friction and extensive adhesive wear often occur when there is a sliding interaction between Ti6Al4V and other engineering materials. In addition, low-amplitude oscillations at the component interfaces cause fretting wear, e.g., at the blade/disk interfaces of fan and compressor stages in turbine engines [9, 10].

The risk of component damage and the need for complex shape modification makes it necessary to use less conventional manufacturing methods. One such method is direct metal laser sintering (DMLS). The DMLS method is one of the varieties of additive manufacturing (AM). It has been developed and improved over the years to ensure that the obtained material properties would be similar to those obtained by conventional methods such as forming, casting, and machining. In contrast to these methods, DMLS makes it possible to produce parts of unusual, technologically complex shapes. These include parts with complex geometries, particularly those having inside empty spaces that are unreachable for the cutting tools and where the use of casting and forging is problematic [7, 11]. However, the properties of the surface layer of Ti6Al4V alloy fabricated by DMLS differ in terms of microstructure, internal stresses, texture, and porosity.

TABLE I

Characteristics of the deposition process for analysed coatings.

Coating	Disk and coating material proportion	Chemical composition (EDS) [at.%]
AlTiN	3× TiAl70 (70 points Al) 1×Ti	27.4% Ti, 31% Al, 41.6% N
TiAlN	3× TiAl60 (60 points Al) 1×Ti	42.7% Ti, 34.3% Al, 23% N

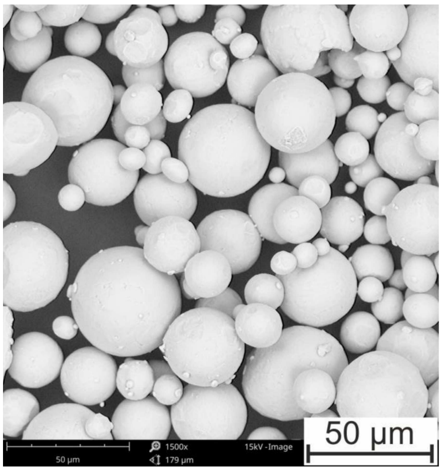

Fig. 1. Size and morphology of Ti6Al4V titanium alloy feedstock powder (SEM).

Therefore, the objective of this study was to determine the relationship between the microstructure, morphology, and mechanical properties of the surface layer of direct metal laser sintered Ti6Al4V alloy and the adhesion of physical vapour deposition (PVD) nitride coatings. The adhesive bond between the coating and the substrate, as well as the relationship between their mechanical properties, such as hardness and elastic modulus, are crucial in this respect.

2. Materials and methods

Specimens of Ti6Al4V alloy fabricated by two different techniques were used as a substrate material. One group of specimens was manufactured in a conventional (Convl.) way from the annealed wrought bars with a diameter of 25 mm. The other group were disks with a 32 mm diameter produced by the DMLS method from laser-sintered powder using the EOSINT M 280 system. After that, two PVD coatings, namely AlTiN and TiAlN, were deposited on the titanium alloy specimens by magnetron sputtering.

The declared chemical compositions of both materials were similar and compliant with ASTM F1472 [12] and ASTM F2924 [13]. The semi-product for DMLS was the gas-atomized powder, EOS Ti64. According to the manufacturer's specifications [14], the powder particle size for 99.7 wt% should not exceed 63 μm (Fig. 1). The sintering process was performed using a 200 W laser in an argon atmosphere, according to the optimal parameters recommended by the EOS manufacturer. The laser exposure speed was 1250 mm/s, the laser beam diameter was 100 μm, and the thickness of a single sintered layer was 30 μm. After direct metal laser sintering, the samples attached to the working plate (also made of Ti6Al4V) were separated from the base plate using a belt cutter.

Next, the cut faces of both types of alloy specimens were machined on the ATM Saphir 550 grinder and polisher. The grinding process was carried out using abrasive disks with grit sizes 120, 220, 500, and 1200. Polishing was conducted with the use of polishing cloths and diamond slurry with a grain size of 3 μm first and then with the use of colloidal silica with a grain size of 0.04 μm. Following rough cleaning and degreasing in a biological wash, the polished surfaces were subjected to ultrasonic cleaning in reverse osmosis water.

Next, the PVD coatings were deposited by magnetron sputtering on the surfaces of the samples. The coating material was obtained from the disks put on the cathode in the proportions specified in Table I. Prior to sputtering, after the samples were put in the chamber, they were preheated to 400°C and ion etched with the 100 V direct current at 20 A, as well as with the amplitude modulated current with the frequency of 240 kHz. The sputtering process was performed in a vacuum below 10^{-9} mbar in an argon and krypton atmosphere.

The technological parameters were selected based on the guidelines specified in the deposition machine manual for a routine industrial coating process for cutting tools. This approach makes it possible to produce prototype parts without running the entire costly process with an incomplete vacuum chamber. Modification of the parameters optimized by the manufacturer is beyond the scope of this study. Only polished disks without any additional surface layer modification by magnetron sputtering were used as the reference samples.

The microstructures of titanium alloy samples were examined using the ZEISS Axio Observer Z1 optical microscope. The microstructures of deposited ceramic coatings were examined with FEI's high-resolution scanning electron microscope Quanta 650 FEG. Imaging was conducted in the voltage range of 2.5–30 kV in a high vacuum, with the working pressure ranging from 2–4 $\times 10^{-3}$ Pa. Most analyses were surface topography observations conducted with the use of the Everhart–Thornley detector (ETD).

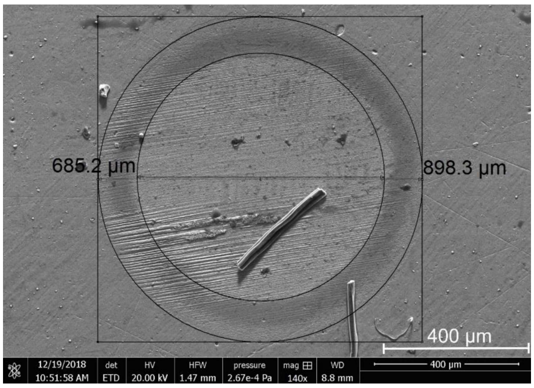

Fig. 2. Example of coating thickness measurement by Calotest (SEM).

Surface topography examinations were conducted with the use of the Bruker ContourGT optical profiler. The surface examination was made for $0.1\times$ 0.1 mm^2 areas. The surface roughness parameter Sa (arithmetical mean height) was calculated.

Internal stresses were measured by the X-ray powder diffraction and $\sin^2(\psi)$ method. X-ray powder diffractograms were captured with the X'Pert^3 powder diffractometer from Philips. XRPD analyses were performed with a copper anode X-ray tube ($\lambda_{\mathrm{Cu}K_\alpha}$ = 1.54178 Å) operating with 30 mA at 40 kV, as well as a bent graphite monochromator. Measurements were made by the continuous method for the 2θ angular range from 10 to 150° with a step of 0.02°. The incident beam slit was 1°, and the deflected beam slit was 1°. To limit the beam divergence, Soller 0.03 mm slits were also used.

Coating thickness was measured by the ball crater test (Calotest) according to PN-EN 1071-2:2003 [15]. The test was carried out with a rotational speed of 400 rev/min for 5 min. A ball with a 25 mm of diameter was used in the test. These parameters made it possible to obtain visible circles that could be measured via SEM (see Fig. 2).

Next, coating nanohardness was measured by the Oliver–Pharr method (Q&P) [16]. The measurements were made in compliance with PN-EN ISO 14577-1 [17] using Anton Paar's ultra nanoindentation tester (UNHT). The surface layer of the test samples was examined with the Berkovich diamond tip. The load in the test was increased with a steady rate of 100 mN/min the moment the indenter came into contact with the examined surface until the force $F_{\max}$ was reached. For the contact to take place, one of the following conditions had to be met: the limit rigidity had to exceed 150 μN/μm, or the limit contact force had to exceed 0.05 mN. The force $F_{\max}$ was maintained for 5 s, and then the indenter was unloaded at a steady rate of 100 mN/min. The force F and the indenter penetration depth h were measured. At least 30 tests per test sample were carried out with force $F_{\max}$ of 20 mN.

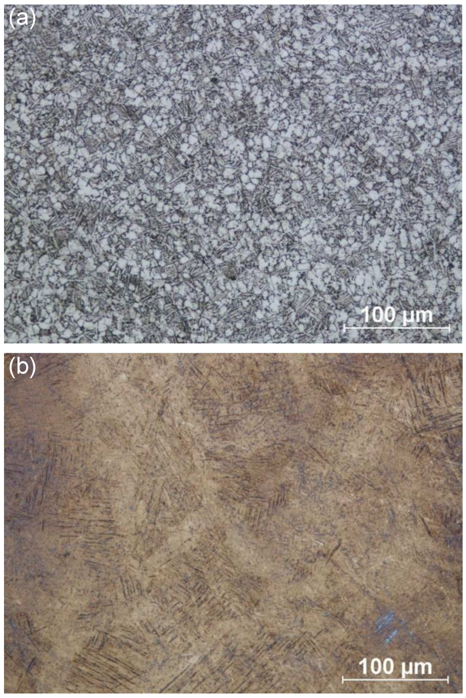

Fig. 3. Microstructure of Ti6Al4V alloy: (a) conventionally manufactured sample (Convl.), (b) DMLS sample.

Coating/substrate adhesion was examined via scratch testing carried out according to ASTM C1624-05 [18], with an increasing normal force on the tested surface. The scratch tests were carried out on Anton Paar's Micro Combi Tester (MCT), using the Rockwell indenter with a fillet radius of 100 μm. The tests were performed over the measuring length of 3 mm with the steadily increasing force ranging from 0.03 to 30 N. The displacement rate was 1 mm/min. In the test there were measured the following parameters: normal force F_n, friction force F_t, friction coefficient μ, penetration depth P_d, and acoustic emission A_E. Following the scratch test, optical microscopy was used to capture the entire scratch track as a panorama. Coating damage stages were identified via images and analysis of characteristic peaks in the acoustic emission diagram. The critical load L_{cr} causing coating failure was defined as a force corresponding to the first visible peaks in the acoustic emission diagram. Then the optical microscopy images were used to verify the location of characteristic peaks A_E. Given no clear boundaries of L_{c1} and L_{c2}, the previous studies usually use one limit value of coating detachment as a criterion for thin coating adhesion assessment [1, 3].

3. Results and discussion

The microstructures of the analysed alloys (used as substrates) are shown in Fig. 3. The conventionally fabricated alloy (Fig. 3a) has an equiaxed,

TABLE II

Roughness of fabricated samples.

	Convl.	DMLS	Convl./AlTiN	DMLS/AlTiN	Convl./TiAlN	DMLS/TiAlN
Sa [μm]	0.040	0.014	0.038	0.027	0.053	0.028

TABLE III

Phase identification results.

Sample	Phase	Figure no.
DMLS	α-Ti (hexagonal lattice, $a = 0.2937$ nm, $c = 0.4652$ nm)	4
Convl.	α-Ti (hexagonal lattice, $a = 0.2937$ nm, $c = 0.4652$ nm) β-Ti (cubic lattice, $a = 0.3309$ nm)	5
DMLS/AlTiN	α-Ti (hexagonal lattice, $a = 0.2937$ nm, $c = 0.4652$ nm) $Al_{0.5}Ti_{0.5}N$ (cubic lattice, $a = 0.419$ nm)	6
Convl./AlTiN	α-Ti (hexagonal lattice, $a = 0.2937$ nm, $c = 0.4652$ nm) $Al_{0.5}Ti_{0.5}N$ (cubic lattice, $a = 0.419$ nm)	7
DMLS/TiAlN	α-Ti (hexagonal lattice, $a = 0.2937$ nm, $c = 0.4652$ nm) $Al_{0.35}Ti_{0.65}N$ (cubic lattice, $a = 0.41805$ nm)	8
Convl./TiAlN	α-Ti (hexagonal lattice, $a = 0.2937$ nm, $c = 0.4652$ nm) $Al_{0.35}Ti_{0.65}N$ (cubic lattice, $a = 0.41805$ nm)	9

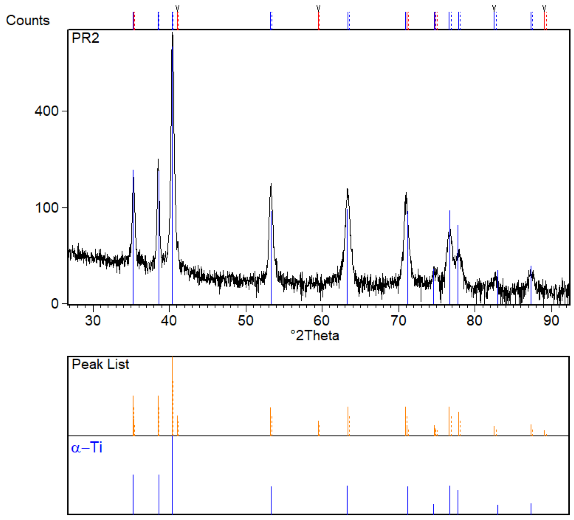

Fig. 4. X-ray powder diffractogram of the DMLS sample.

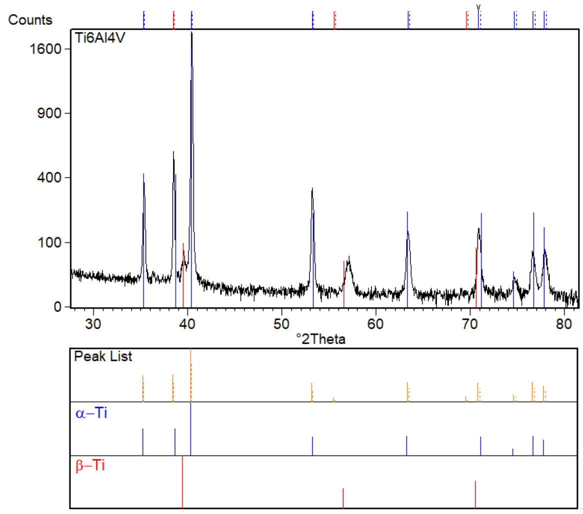

Fig. 5. X-ray powder diffractogram of the Convl. sample.

globular microstructure due to recrystallization. The phases α and β are clearly visible. The polished section of the DMLS alloy (Fig. 3b) shows the lamellar martensitic structure α' that was formed as a result of fast cooling from the annealing temperature of the β phase [19, 20].

As follows from the analysis of the arithmetical mean height Sa results (Table II), it is below 0.1 μm. It can be also observed that all DMLS substrate samples have lower values of the surface roughness parameter Sa than the conventional substrate samples. Given the lower surface roughness, it can be assumed that the additive-manufactured samples will thus exhibit improved fatigue strength and increased fretting resistance compared to the conventional samples. As mentioned in [21], for the surface roughness below Sa = 0.1 μm, this effect can be insignificant compared to other factors.

The phase composition results are given in Table III and in Figs. 4–9. For the Convl. sample, two phases were identified, i.e., α-Ti and β-Ti. The analysis of the XRD results for the DMLS sample in Fig. 4 demonstrates that all peaks can be identified as α/α'. Given that α and α' have the same hexagonal close-packed (hcp) crystal structure, it is difficult to identify peaks even though they are

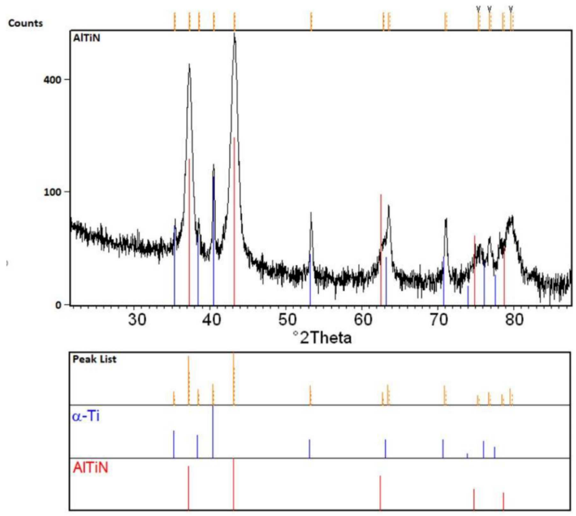

Fig. 6. X-ray powder diffractogram of the DMLS/AlTiN sample.

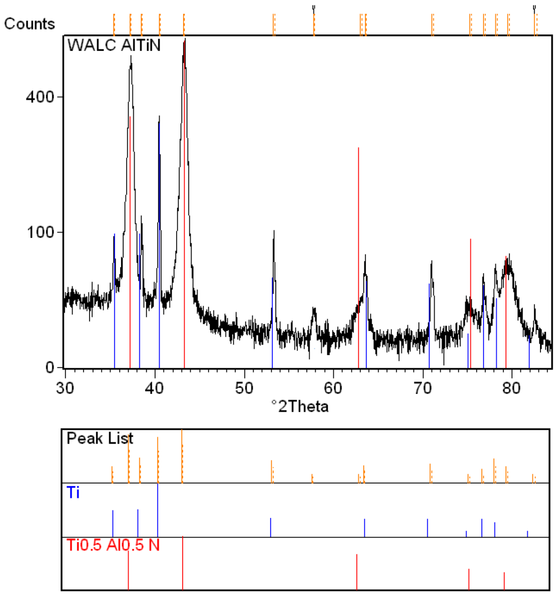

Fig. 7. X-ray powder diffractogram of the Convl./AlTiN sample.

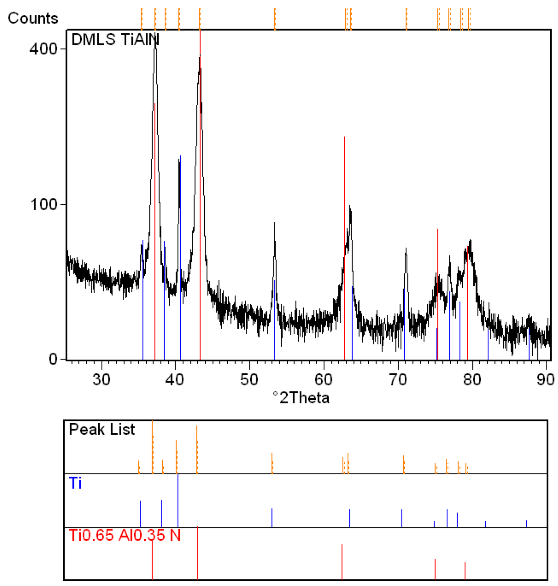

Fig. 8. X-ray powder diffractogram of the DMLS/TiAlN sample.

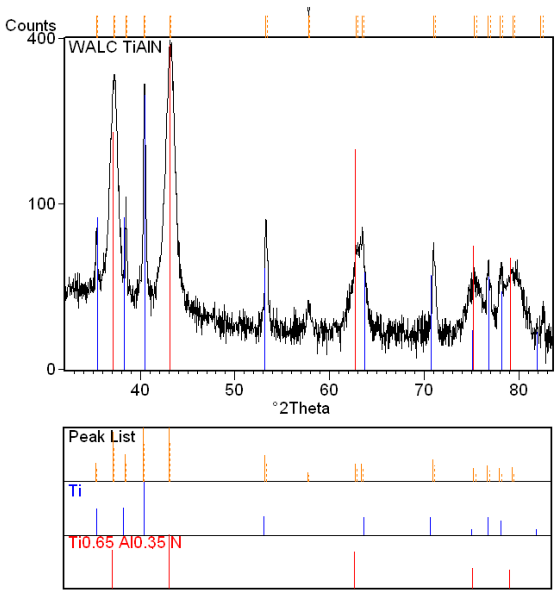

Fig. 9. X-ray powder diffractogram of the Convl./TiAlN sample.

two different phases. The XRD results of the DMLS samples do not show the presence of the β phase peak, which may be proof of martensitic microstructure. The peaks identified in this region correspond to the hexagonal phase with the lattice parameters $a = 0.293$ nm and $c = 0.465$ nm, with the values showing agreement with those reported in the literature [22] for the martensitic phase. In addition, according to [23], the cooling rate of DMLS for the Ti6Al4V powder products is 10^6 K/s, which causes a change of α into α'.

The location of diffraction reflexes in the samples with AlTiN and TiAlN coatings (Figs. 6–9) indicates the presence of two phases, i.e., $Al_{0.5}Ti_{0.5}N$ (cubic lattice, $a = 0.419$ nm) and $Al_{0.35}Ti_{0.65}N$ (cubic lattice, $a = 0.41805$ nm). Both phases have the same type of crystal lattice (cubic lattice with stitial Al and Ti atoms and interstitial N atoms). The samples Convl./AlTiN and Convl./TiAlN show the presence of additional diffraction reflexes that have not been assigned to any of the above phases.

The penetration depth of X-rays for the PVD coatings ranges from 11 to 42.7 μm depending on the incidence angle θ. Internal stresses were determined for two phases, i.e., α-Ti and TiAlN (general notation TiAlN was used for the phases $Al_{0.5}Ti_{0.5}N$ and $Al_{0.35}Ti_{0.65}N$). The interplanar spacing d_{hkl} as

TABLE IV

Internal stresses for test samples.

Sample	Phase	Miller indices hkl of diffraction line	Angle 2θ [°] at $\sin^2(\psi) = 0$	Penetration depth [μm] at $\sin^2(\psi) = 0$	$\frac{E}{(1+\nu)}$ [GPa]	Internal stresses [GPa] (stand. dev. in brackets)
Convl.	α-Ti	(213)	140.750	15.5	85	−0.239 (0.055)
DMLS	α-Ti	(213)	140.780	15.5	85	−0.535 (0.002)
DMLS/AlTiN	α-Ti	(213)	140.771	15.5	85	−0.334 (0.002)
	AlTiN	(422)	130.104	38.8	318	−2.360 (0.150)
Convl./AlTiN	α-Ti	(213)	140.742	15.5	85	−0.144 (0.170)
	AlTiN	(422)	130.102	38.8	318	−2.189 (0.003)
DMLS/TiAlN	α-Ti	(213)	140.749	15.5	85	−0.289 (0.005)
	TiAlN	(422)	129.604	38.7	318	−3.167 (0.030)
Convl./TiAlN	α-Ti	(213)	140.752	15.5	85	−0.213 (0.005)
	TiAlN	(422)	129.603	38.7	318	−3.094 (0.020)

TABLE V

Calotest thickness results for test samples.

Coating type	Mean thickness S_p [μm]	Std. dev [μm]
Convl./TiAlN	7.33	0.12
DMLS/TiAlN	7.31	0.14
Convl./AlTiN	7.37	0.15
DMLS/AlTiN	7.35	0.14

a function of the $\sin^2(\psi)$ angle was measured along the diffraction line (213) for the α-Ti phase and along the diffraction line (422) for the TiAlN phase. The distance d_n was determined based on the XRD measurements for the angle of $\psi = 0$. The measurement results are given in Table IV.

The comparison of the internal stresses has shown that the compressive stress of the DMLS material is 124% higher than that of the conventional material. The compressive stresses in the DMLS coatings are 2–13% higher than those in the conventional coatings.

The coating thickness results obtained from the Calotest are given in Table V. All PVD coatings exhibit a similar mean thickness, irrespective of the substrate type.

The results of hardness and elastic modulus, as well as the mean values of the $H_{\text{coating}}/E_{\text{coating}}$ ratio and the $H^3_{\text{coating}}/E^2_{\text{coating}}$ plasticity index, are given in Table VI.

According to [24, 25], the $H_{\text{coating}}/E_{\text{coating}}$ ratio (elastic strain to failure) can be used as a measure of wear initiation. A higher value of the $H_{\text{coating}}/E_{\text{coating}}$ ratio indicates higher resistance of a coating to abrasive wear and elastic deformation. Nonetheless, it is necessary to avoid extreme misfits between the coating and the substrate due to applications for PVD coatings [25]. According to [26], higher values of the ratios $H_{\text{coating}}/E_{\text{coating}}$ and $H^3_{\text{coating}}/E^2_{\text{coating}}$ should result in higher resistance to abrasive wear; however, this principle does not necessarily hold true when the very same coating is deposited on different substrates [27]. For coatings, the $H_{\text{coating}}/E_{\text{coating}}$ ratio is, on average, ~0.05. The $E_{\text{coating}}/E_{\text{substrate}}$ ratio is 20–30% lower for the coatings deposited on the DMSL substrate, which indicates a better fit between their elastic moduli.

Taking the above into consideration, it can be claimed that the type of manufacturing technique (DMLS/Convl.) has no statistically significant effect on the hardness and elastic modulus of ceramic nitride coatings deposited on the analysed titanium alloy. Also, the obtained values of the mechanical parameters of the coatings are comparable to those reported in the literature for other substrates [28].

The scratch test results were analysed for the critical load $L_{cr.}$ The acoustic emission A_E (panels (a) in Figs. 10–13) was used to identify the location of the damage. First, the location of characteristic peaks signalling the critical load of a coating was identified, and then the location was verified based on the optical microscopy images. The results are given in Table VII. It can be observed that all coatings deposited on the DMLS substrate have a 25% higher adhesion than those deposited on the conventionally manufactured alloy. The critical load L_{cr} of the AlTiN coating deposited on the Ti6Al4V alloys (irrespective of the substrate manufacturing method) is over 20% lower than for the TiAlN coatings, which have similar values of L_{cr}. Based on the Shapiro–Wilk test, we can assume a zero hypothesis H_0 with the normal distribution for $\alpha = 0.05$, which may indicate high homogeneity of the coatings. The Grubbs test statistics [29, 30] do not show any outliers that would indicate a gross error for the same assumed significance level of $\alpha = 0.05$ (Table VII).

TABLE VI

Mean hardness and elastic modulus of surface layer, and their ratios for test samples. According to the standard PN-EN ISO14577-1 [17], the subscript IT is explained as instrumented indentation.

Coating	–	–	AlTiN	AlTiN	TiAlN	TiAlN
Substrate: Ti64	DMLS	Convl.	DMLS	Convl.	DMLS	Convl.
H_{IT} [GPa]	5.7 ± 0.2	4.8 ± 0.4	25.0 ± 4.6	26.1 ± 4.3	23.6 ± 3.4	23.2 ± 3.3
E_{IT}[GPa]	137.0 ± 4.1	114.5 ± 4.7	518.7 ± 129.1	559.2 ± 117.3	411.4 ± 45.8	503.5 ± 99.4
$H_{\text{coating}}/E_{\text{coating}}$	–	–	0.048	0.047	0.057	0.046
$H^3_{\text{coating}}/E^2_{\text{coating}}$	–	–	0.059	0.057	0.078	0.049
$E_{\text{coating}}/E_{\text{substrate}}$	–	–	3.79	4.88	3.00	4.40

TABLE VII

The L_{cr} results obtained from the scratch test.

coating	substrate	L_{cr} [N]	Shapiro–Wilk test		Grubbs test statistics	
			W	p	W	p
AlTiN	DMLS	16.96 ± 3.35	0.9814	0.9887	2.0104	0.3253
AlTiN	Convl.	12.83 ± 2.18	0.8743	0.1095	1.7017	0.8701
TiAlN	DMLS	21.95 ± 2.22	0.9806	0.9677	1.6925	0.5968
TiAlN	Convl.	16.38 ± 3.16	0.9648	0.8552	1.7398	0.4141

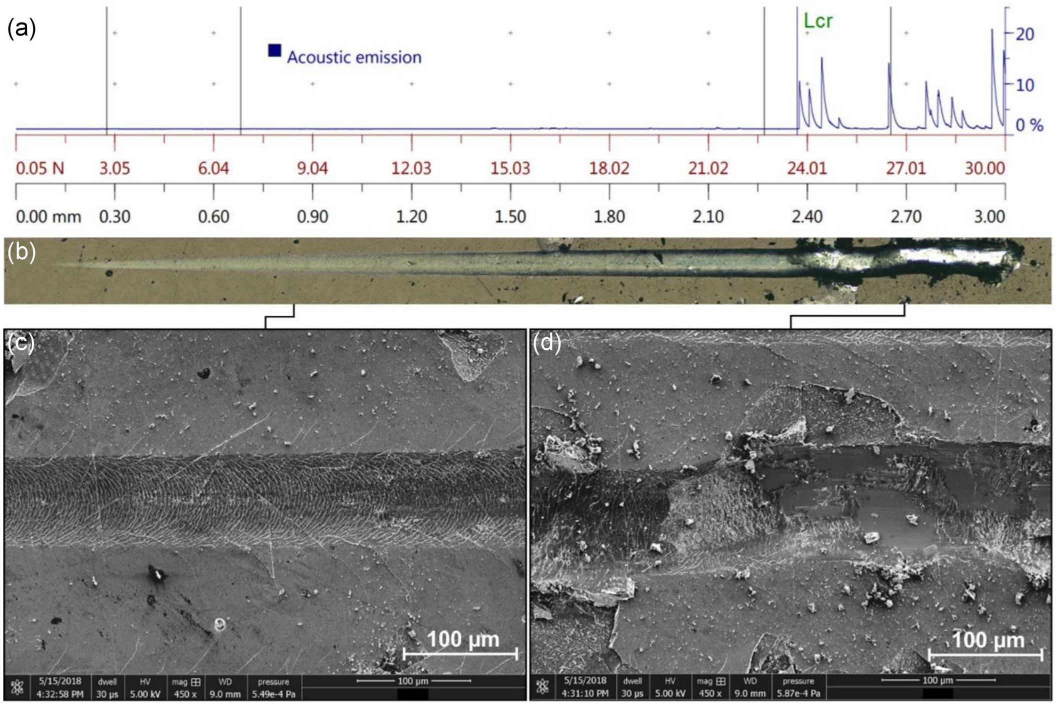

Fig. 10. Scratch of the AlTiN coating deposited on the DMLS substrate. Acoustic emission (a), OM image of scratch panorama (b), SEM images of: conformal cracks (c), exposed substrate beyond L_{cr} boundary (d).

Panels (b) in Figs. 10–13 show the OM images of scratch panoramas obtained with the Anton Paar MCT, and (panels (c) and (d) in Figs. 10–13) the SEM images of characteristic spots for the selected tests. The AlTiN and TiAlN coatings have characteristic conformal microcracks in the middle of the scratch (panels (c) in Figs. 10–13). Conformal cracks are formed as a result of coating response to

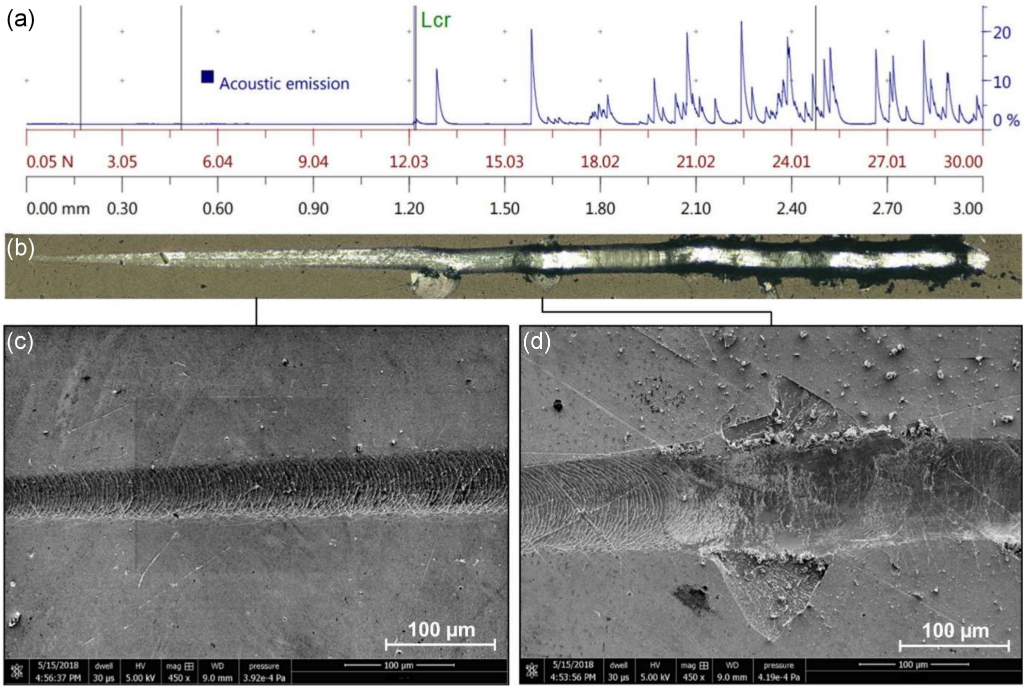

Fig. 11. Scratch of the AlTiN coating deposited on the conventionally fabricated substrate. Acoustic emission (a), OM image of scratch panorama (b), SEM images of: conformal cracks (c), substrate-exposing spalling (d).

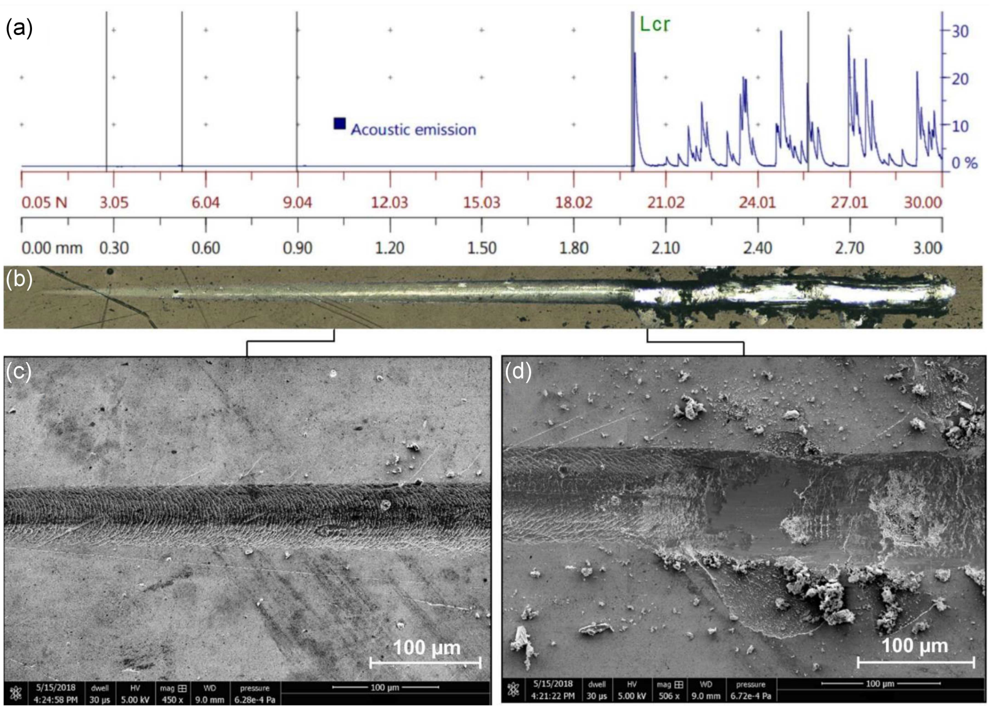

Fig. 12. Scratch of the TiAlN coating deposited on the DMLS substrate. Acoustic emission (a), scratch panorama under optical microscope (b), SEM images of: conformal cracks (c), L_{cr} boundary (d).

scratching and are in the form of cohesive damage. They occur together with brittle cracks caused by tension (chevron cracks) [5, 26, 31]. The adhesive damage L_{cr} of the above coatings was usually connected with the presence of characteristic spalling shown in panels (d) in Figs. 10-13 and the trapping of the coating between the indenter and the substrate in the final stage of substrate exposure.

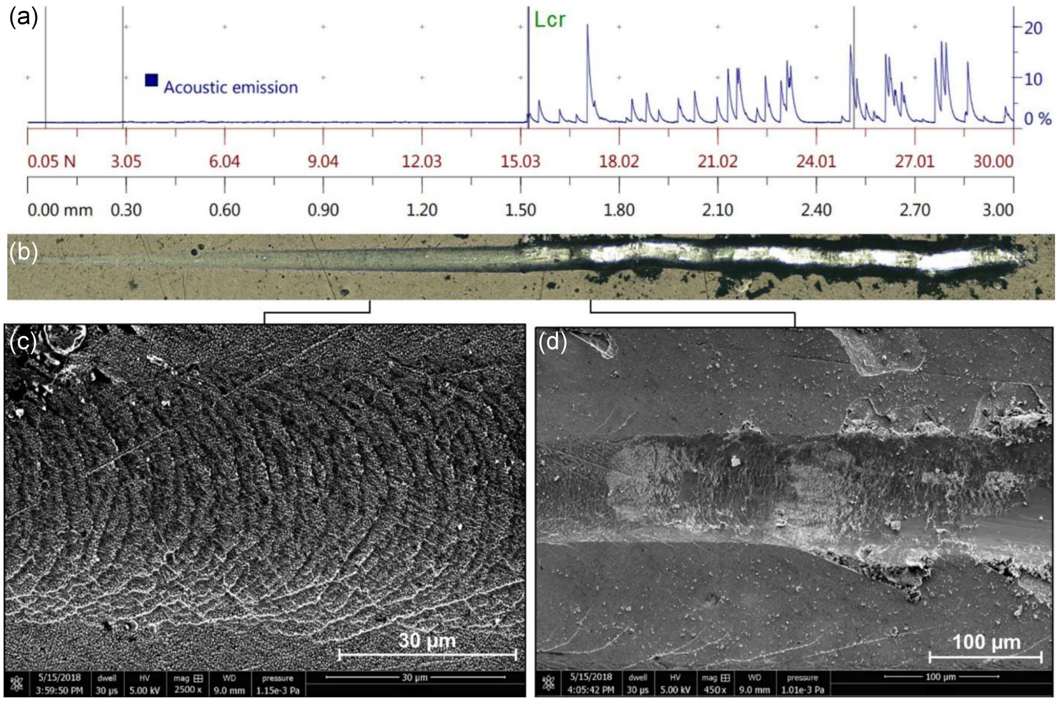

Fig. 13. Scratch of the TiAlN coating deposited on the conventionally fabricated substrate. Acoustic emission (a), OM image of scratch panorama (b), SEM images of: conformal cracks (c), L_{cr} boundary (d).

4. Conclusions

Concluding, it can be stated that the type of surface layer is of significant importance for coating/substrate adhesion. Hence, PVD coatings deposited on the direct metal laser sintered substrate exhibited much higher adhesive properties, which resulted predominantly from a better fit of the $E_{\mathrm{coating}}/E_{\mathrm{substrate}}$ ratio and higher compressive stresses. The results of this study lead to the following conclusions:

1. Phase composition examination showed that the tested Ti6Al4V alloys had different phase structures. The DMLS alloy had a martensitic phase α'. On the other hand, the alloy fabricated by a standard metallurgical process had a two-phase structure of $\alpha + \beta$.

2. Microscopic examination showed that a conventionally produced alloy had an equiaxed, globular grain structure that was formed as a result of recrystallization. In this structure, there were observed two phases, namely, α and β. In contrast, the polished section of the DMLS alloy had a lamellar martensitic α' phase caused by fast cooling from the annealing temperature of the β phase. Additionally, the literature review shows that the structure of direct metal laser sintered alloys can depend on the product wall thickness and the distance from the base plate onto which it is printed.

3. All DMLS substrate samples have over 120% higher compressive stresses in the surface layer compared to the samples with the conventionally fabricated substrate. Similarly, all coatings deposited on the DMLS Ti6Al4V alloy substrate had, on average, 2–13% higher compressive stresses compared to the coating deposited on the conventionally fabricated substrate.

4. Surface roughness results demonstrated that all DMLS samples had lower values of the surface roughness parameters Sa than the Convl. ones. It was also observed that the surface roughness parameters Sa were relatively lower for the PVD coatings deposited on the DMLS substrate than for those deposited on the conventionally manufactured substrate.

5. Measurements made by the O&P method did not show statistically significant differences between the mechanical properties (E_{IT} and H_{IT}) of AlTiN and TiAlN coatings deposited on the Convl. and DMLS substrates (IT reads as instrumented indentation according to the nomenclature used in [17]). Moreover, the values of the mechanical parameters of these coatings were comparable to those reported in previous studies on the deposition of such coatings on other metallic and ceramic substrates.

6. As a result of the martensitic structure formation, the direct metal laser sintered alloy had approx. 20% higher nanohardness and

elastic modulus of the surface layer than the alloy produced by a conventional manufacturing process. This led to a better fit between the coating/substrate elastic moduli ratio $E_{\text{coating}}/E_{\text{substrate}}$.

7. The scratch test results showed that all coatings deposited on the DMLS substrate exhibited a nearly 25% higher critical load L_{cr} (which was a measure of adhesion) than those deposited on the conventionally manufactured substrate.
8. The post-scratch test microscopic examination showed that both AlTiN and TiAlN coatings were susceptible to cohesive damage.

References

[1] P. Yi, L. Peng, J. Huang, *Mater. Sci. Eng. C* **59**, 669 (2016).

[2] V. Bonu, M. Jeevitha, V. Praveen Kumar, G. Srinivas, Siju, H.C. Barshilia, *Surf. Coat. Technol.* **387**, 125531 (2020).

[3] R. Niu, J. Li, Y. Wang, J. Chen, Q. Xue, *Surf. Coat. Technol.* **309**, 232 (2017).

[4] D. Morozow, Z. Siemiątkowski, E. Gevorkyan, M. Rucki, J. Matijošius, A. Kilikevičius, J. Caban, Z. Krzysiak, *Materials* **13**, 4687 (2020).

[5] M. Walczak, K. Pasierbiewicz, M. Szala, *Acta Phys. Pol. A* **136**, 294 (2019).

[6] C.-W. Chan, J. Quinn, I. Hussain, L. Carson, G.C. Smith, S. Lee, *Surf. Coat. Technol.* **405**, 126714 (2021).

[7] R. Żebrowski, M. Walczak, *Arch. Metall. Mater.* **64**, 377 (2019).

[8] G. Deng, Y. Chong, L. Su et al., *Tribol. Int.* **169**, 107464 (2022).

[9] C.H. Hager Jr., J. Sanders, S. Sharma, A. Voevodin, *Wear* **263**, 430 (2007).

[10] F. Xue, Z.-X. Wang, W.-S. Zhao, X.-L. Zhang, B.-P. Qu, L. Wei, *Eng. Fail. Anal.* **44**, 299 (2014).

[11] R. Żebrowski, M. Walczak, T. Klepka, K. Pasierbiewicz, *Eksploatacja i Niezawodnosc — Maintenance and Reliability* **21**, 46 (2019).

[12] ASTM F1472: *Standard Specification for Wrought Titanium-6Aluminum-4Vanadium Alloy for Surgical Implant Applications (UNS R56400).*

[13] ASTM F2924: *Standard Specification for Additive Manufacturing Titanium-6 Aluminum-4 Vanadium with Powder Bed Fusion.*

[14] *Material data sheet EOS Titanium Ti64 M290 EOS GmbH — Electro Optical Systems*, 2011, p. 11.

[15] PN-EN ISO 26423:2016: *Fine Ceramics (Advanced Ceramics, Advanced Technical Ceramics) — Determination of Coating Thickness by Crater-Grinding Method.*

[16] W. Oliver, G.M. Pharr, *J. Mater. Res.* **19**, 18 (2004).

[17] PN-EN ISO 14577-1:2015: *Metallic materials — Instrumented indentation test for hardness and materials parameters — Part 1: Test method.*

[18] ASTM C1624-05: *Standard Test Method for Adhesion Strength and Mechanical Failure Modes of Ceramic Coatings by Quantitative Single Point Scratch Testing.*

[19] G.A. Longhitano et al., *J. Mater. Process. Technol.* **252**, 202 (2018).

[20] W.S.W. Harun, N.S. Manam, M.S.I.N. Kamariah, S. Sharif, A.H. Zulkifly, I. Ahmad, H. Miura, *Powder Technol.* **331**, 74 (2018).

[21] W. Grzesik, *Mechanik* **8–9**, 587 (2015).

[22] R. Boyer, G. Welsch, E.W. Collings, *Materials Properties Handbook: Titanium Alloys*, ASM International, 1994.

[23] H.K. Rafi, N.V. Karthik, H. Gong, T.L. Starr, B.E. Stucker, *J. Mater. Eng. Perform.* **22**, 3872 (2013).

[24] W.-J. Shen, M.-H. Tsai, J.-W. Yeh, *Coatings* **5**, 312 (2015).

[25] A. Leyland, A. Matthews, *Wear* **246**, 1 (2000).

[26] M. Szala, M. Walczak, K. Pasierbiewicz, M. Kamiński, *Coatings* **9**, 340 (2019).

[27] M. Łępicka, M. Grądzka-Dahlke, D. Pieniak, K. Pasierbiewicz, K. Kryńska, A. Niewczas, *Wear* **422–423**, 68 (2019).

[28] D. Özkan, M.A. Yılmaz, M. Szala et al., *Ceram. Int.* **47**, 20077 (2021).

[29] A.A. Afifi, V. Clark, *Computer-Aided Multivariate Analysis*, 3rd Ed., Chapman & Hall, 1996.

[30] *Engineering Statistics Handbook*.

[31] R. Manish, J.P. Davim, *Thermal Sprayed Coatings and their Tribological Performances*, IGI Global, 2015.